

Stabilization of single-electron pumps by high magnetic fields

J. D. Fletcher,¹ M. Kataoka,¹ S. P. Giblin,¹ Sunghun Park,² H.-S. Sim,² P. See,¹

T. J. B. M. Janssen,¹ J. P. Griffiths,³ G. A. C. Jones,³ H. E. Beere,³ and D. A. Ritchie³

¹ National Physical Laboratory, Hampton Road, Teddington, Middlesex TW11 0LW, United Kingdom

² Department of Physics, Korea Advanced Institute of Science and Technology, Daejeon 305-701, Korea and

³ Cavendish Laboratory, J J Thomson Avenue, Cambridge CB3 0HE, United Kingdom

(Dated: August 9, 2011)

We study the effect of perpendicular magnetic fields on a single-electron system with a strongly time-dependent electrostatic potential. Continuous improvements to the current quantization in these electron pumps are revealed by high-resolution measurements. Simulations show that the sensitivity of tunnel rates to the barrier potential is enhanced, stabilizing particular charge states. Nonadiabatic excitations are also suppressed due to a reduced sensitivity of the Fock-Darwin states to electrostatic potential. The combination of these effects leads to significantly more accurate current quantization.

PACS numbers: 73.23.Hk, 73.63.Kv

Single-electron devices proposed for quantum information technologies [1–3] and quantum electrical metrology [4–6] feature the capture, manipulation, and release of electrons through a series of gate pulses. To design such devices it is important to understand the electronic response to a rapid time-varying electrostatic potential, often in the presence of externally applied magnetic fields. The effects of magnetic confinement on electronic states [7, 8] and on electron-electron interactions [9] have been studied extensively. However, the effect of magnetic fields on the electron dynamics under time-varying potentials is less established. Semiconductor single-electron pumps in magnetic field are an example of a system which requires a consideration of these effects. It was found that accuracy of the quantization current produced by these devices was strongly enhanced in magnetic fields [10, 11] but the origin of this effect is yet to be explained.

In this Letter we use detailed measurements and numerical models to reveal how perpendicular magnetic fields change the tunneling dynamics of the quasi-bound electrons in a single-electron device – the tunable-barrier electron pump. First we find, through numerical calculations, that magnetic fields enhance the sensitivity of tunnelling rates to the confinement barriers. This is detected through the enhancement in stability of the number of pumped electrons. We then show that magnetic field increases the “stiffness” of the electronic wavefunction against the rapid electrostatic perturbations that arise when operating the pumps at high speed. This protects the trapped electrons from loss through nonadiabatic excitations [12], suppressing this process of *quantum spillage*. Our results also reveal that accurate current quantization is achievable at high magnetic field in these devices, which is crucial for uses in quantum metrology.

Our pumps use a dynamically formed quantum dot defined in a 2DEG AlGaAs/GaAs heterostructure by two surface gates. The gates cross an etch-defined wire terminated with ohmic electrical contacts, shown schematically in Fig. 1(a) [13]. One of the adjustable energy barriers, the *entrance* gate, is repeatedly lowered and raised by modulating the potential by V_{RF} about a constant negative value V_{G1} while holding

the other *exit* gate at a constant negative voltage V_{G2} [14]. This process is illustrated in Fig. 1(b)i-iv: Electrons from the source reservoir are loaded into a quantum dot formed in the space between the gates (i) which is increasingly isolated by the rising entrance barrier. Some initially-trapped electrons escape back through this rising barrier before tunneling is cut off completely (ii). These back-tunneling rates Γ_n vary dramatically for different charge number n due to the charging energy. This leads to the trapping of the same number of electrons in each cycle, and is the mechanism for quantisation of charge transport in this type of pump (iii). Electrons that remain trapped are forced over the exit barrier into the drain lead (iv), producing a current in an external circuit [15]. The number of electrons pumped by the dot can be changed by adjusting the values of V_{G1} and V_{G2} giving current plateaux at integer multiples of ef , where f is the operating frequency. Broadly speaking, V_{G2} controls the number of electrons trapped after stage ii, while V_{G1} determines how many of these electrons are emptied into the drain [16].

Figure 1(c) shows measurements of the output current of a pump operating at a frequency $f = 400$ MHz performed in a ^3He cryostat with a base temperature of ~ 300 mK. Data is shown for magnetic fields up to 14 T in 2 T steps, concentrating on the plateau at $I = ef$ (i.e. $n = 1$) visible over a range of exit gate V_{G2} (data have been offset for clarity). This reveals both a sharpening of the transition region and a lengthening of the current plateaux in magnetic field similar to that seen previously [10, 11], reducing errors in pump operation.

The movement of plateaux boundaries in magnetic field is shown in Fig. 1(d) (this was subtracted in Fig. 1(c) where data are aligned to the edge of the second plateau). This shift in position has been linked to magnetic confinement [17]; a reduction in tunnel rate is compensated by a reduction in V_{G2} giving the same pump current. We have performed detailed high resolution measurements [18] on this device as shown in Fig. 1(e). We zoom in on the plateau, expanding the current scale by a factor 4,000. This shows that the magnetic field brings the pumped current continuously closer to the expected value of ef (corresponding to exactly one electron pumped

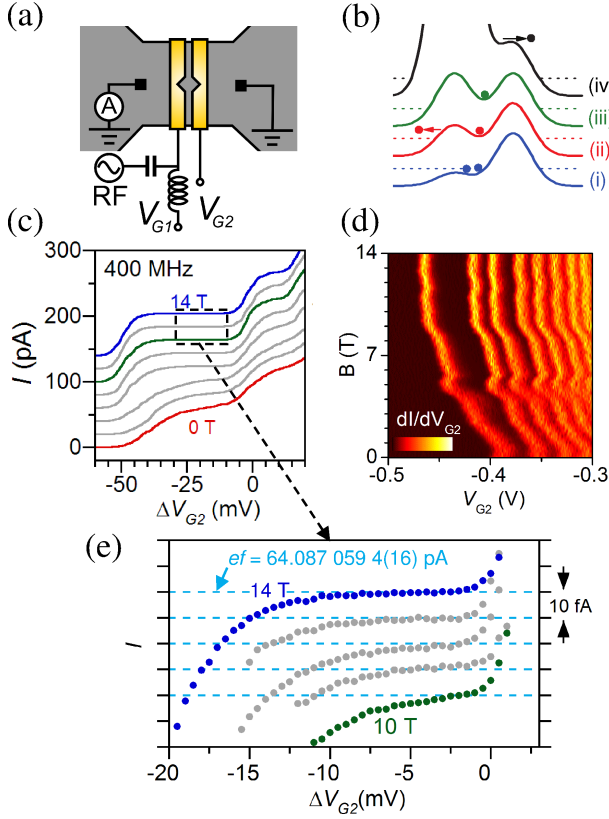


FIG. 1: (a) Schematic of the pump. Left (entrance) gate is modulated by an R.F. source via a bias-tee. Channel width: $1\text{--}2\mu\text{m}$, gate width (separation) 200 nm (50 nm). (b) Potential profile during the pumping cycle offset vertically: i. loading, ii. back-tunneling, iii. trapping, iv. ejection. (c) Pump current at $f = 400\text{ MHz}$ as a function of V_{G2} showing $I = ef, 2ef$ plateaux. (d) dI/dV_{G2} as a function of V_{G2} and magnetic field. (e) High resolution scans of the $I = ef$ plateau at $f = 400\text{ MHz}$ at $10, 11, \dots, 14\text{ T}$. Data and the ef value (dashed lines) are offset for clarity

per cycle) even at the highest fields accessible with our experimental system. Now we focus upon the relationship between the measured pump current and the electronic wavefunction in the dynamic quantum dot and how these are affected by the introduction of a magnetic field.

The pumped current is determined by the back-tunneling of excess electrons before the dot is isolated from the leads [6, 19] where the entrance barrier is rising rapidly as in Fig. 1(b) ii. The key parameters are the time-dependent tunnel rates Γ_n out of the dot, as determined by the confining geometry [19]. The separation of lifetimes between states that differ by one electron $\Gamma_n \ll \Gamma_{n+1}$, combined with the increasing opacity of the tunnel barrier leads to the mean number of electrons captured $\bar{n} \simeq \text{an integer}$. The effect of magnetic field can be investigated by calculating $\Gamma_n(B)$ for a model of the confinement potential.

We have calculated the tunnel coupling for a two-dimensional potential well based on the experimental configuration in a magnetic field. The broadening of the dot levels are calculated by the lattice Green's function method [20, 21].

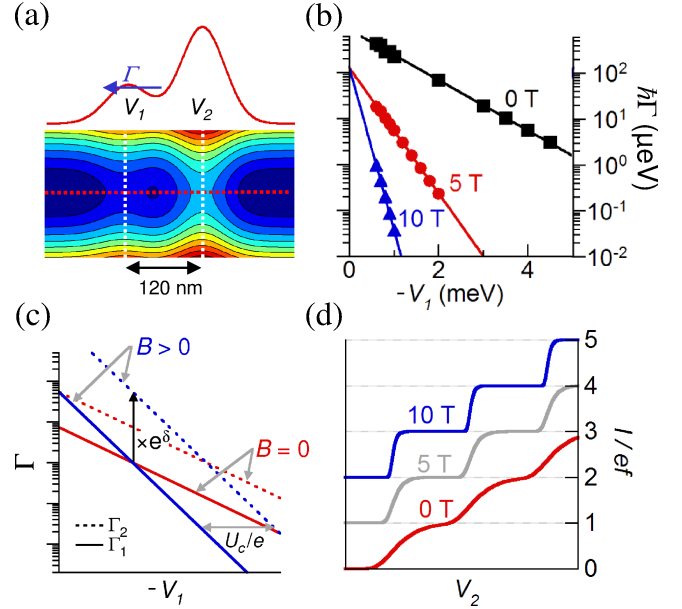


FIG. 2: Model calculations: (a) Contour plot of the model 2D potential well. Vertical lines indicate the positions of the gate-defined barriers. Line cut is through the symmetry point indicated by the dashed red line. The calculated tunnel rate Γ is for electrons tunneling back to the source lead (as indicated). (b) Tunnel rate from the potential well as a function of V_1 , the entrance barrier for different values of applied magnetic field for a constant $V_2 = 50\text{ meV}$. Solid lines are fits to an exponential function. (c) Increase in the relative escape rate between $n = 1$ and $n = 2$ states in finite field due to magnetic confinement. (d) Calculated pump current as a function of control voltage in the back-tunneling model [19] with the effects of a magnetic field (offset vertically).

The two-dimensional continuous system is modeled by a discrete square lattice with a tight-binding Hamiltonian. The on-site energies of the Hamiltonian contain the position-dependent potential, while off-diagonal elements, describing the hopping between neighboring sites, include the Peierls phase factor from the magnetic field. The entrance and exit barriers are modeled by Gaussian functions (width 60 nm , separation 120 nm , height V_1 and V_2 respectively) as shown in Fig. 2(a). Lateral confinement (perpendicular to the pumping direction) is provided by a parabolic potential. Parameters were chosen to approximate the experimental geometry and give an orbital energy level spacing similar to that found from the excitation spectrum of the quantum dots in our pumps [12, 22].

Figure 2(b) shows the back-tunnel rate as a function of V_1 for a fixed exit barrier height $V_2 = 50\text{ mV}$. This shows the expected exponential variation at all fields but with a reduction in the overall tunnel coupling at higher fields – the dot is increasingly decoupled from the leads by magnetic confinement. This is expected to shift the operating point of the pump at higher fields as shown above [17]. In addition, the sensitivity of Γ to the barrier height (i.e. the slope of the fits in Fig. 2(b)) is strongly enhanced in higher magnetic fields. We

show below that this is responsible for enhanced quantization.

We fit the tunnel rate to the expression $\Gamma = \Gamma_0 \exp[E_b/\epsilon(B)]$ where E_b is the difference in energy between the dot level and the barrier V_1 and $\epsilon(B)$ is a field-dependent parameter characterizing the barrier/dot geometry. We take $E_b = -eV_1 - E_n$ where $E_n = E_0(V_1, V_2) + (n-1)U_c$, i.e. a single electron energy plus a charging energy U_c for each additional electron. $\epsilon(B)$ can then be extracted from the numerical calculations of $\Gamma(V_1)$ shown above.

We find that $\epsilon(B)$ is reduced by a factor 6 between $B = 0$ T and 10 T, increasing the relative tunnel rates $\delta = \ln(\Gamma_{n+1}/\Gamma_n)$ by the same factor. This is shown schematically in Fig. 2(c) where the V_1 (\approx linear in time on the scale of this process) dependence of the decay rates for dots with n (solid lines) and $n+1$ electrons (dotted lines) is plotted. The enhanced sensitivity to barrier height is caused by magnetic confinement of the wavefunction at high field; at fields of $B \approx 10$ T the wavefunction is largely confined to a region of only ≤ 30 nm across so the electron wavefunction must be forced very close to the barrier to give any appreciable tunnel coupling. In this regime the probability density is so concentrated that small variations in barrier height change the tunnel-coupling very rapidly. In comparison, at low field, the tunnel coupling varies more slowly and the process of decoupling the dot states from those in the leads is more gradual.

Enhancing the ratio of tunnel rates between $n+1$ and n electron states will increase the stability of the number of trapped charges. We show this in Fig. 2(d) where we plot the calculated pump current $I(V_2)$ according to a rate equation model describing the back-tunneling process [19], but including the field dependence of $\epsilon(B)$ found above. This predicts a sharpening of the plateau transitions like that seen experimentally (e.g. Fig. 1(a)). This model assumes that the dot initially contains several more electrons than the final number pumped but due to the enhanced tunnel rates for higher n all memory of the initial charge state is erased by the rapid decay of these states [19]. The functional form of $I(V_2)$ arises from changes in the dot energy levels as V_2 is varied. The electronic wavefunction is “squeezed” against the entrance barrier, tuning the overall tunnel coupling. On plateaux this is set so that the $n+1$ state is fully emptied on the time scale of the changes in barrier height, leaving n electrons trapped. In between plateaux this process is incomplete and the number of electrons trapped fluctuates.

The confinement effect described above increases the range of V_2 over which the unstable state is essentially fully emptied. This effect alone gives a longer current plateaux. However, the dependence of tunnel rates on V_2 is also sensitive to magnetic confinement effects; tunnel rates are more sensitive to V_2 at high field giving a re-scaling of $I(V_2)$. The net effect is plateaux of the same length in the control parameter V_2 but with much sharper boundaries. Experimentally both sharpening and lengthening of current plateaux in magnetic field have been observed in devices of different design. Increases in the charging energy alone could cause lengthening but we do not expect that the charging energy to change by as much

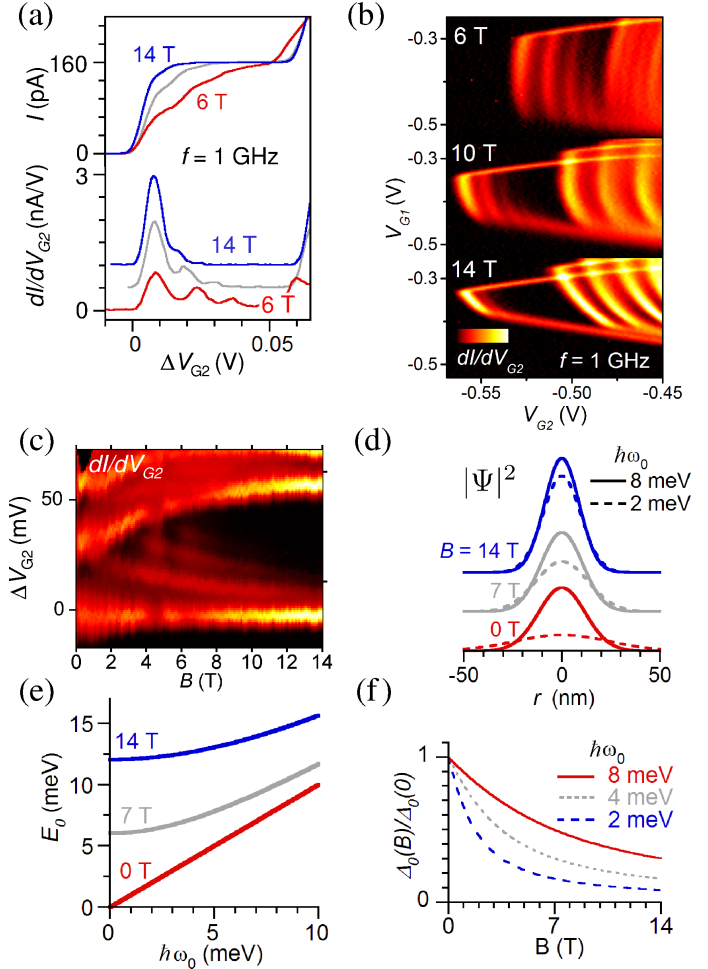


FIG. 3: (a) Current plateaux at 1 GHz for fields of 6, 10 and 14 T along with dI/dV_{G2} (offset vertically). (b) Maps of dI/dV_{G2} (color scale) as a function of both V_{G2} and V_{G1} for 6 T, 10 T and 14 T. (c) Color map of dI/dV_{G2} as a function of field up to 14 T. (d) Fock-Darwin state probability density for different combinations of magnetic field and electrostatic confinement ($\hbar\omega_0 = 2$ meV and 8 meV are shown with dashed and solid lines respectively.) (e) Eigenenergies of the ground state solution of the Fock-Darwin confinement potential for different combinations of magnetic field strength and electrostatic confinement energy ω_0 . (f) Field dependence of the first excitation gap ($n, l = 0, 0$ to $n, l = 0, 1$ where n, l are the radial quantum number and orbital angular momentum respectively) for $\hbar\omega_0 = 2, 4, 8$ meV.

as a factor of two, as observed experimentally. An alternative explanation is that the rescaling effects described above are not identical for V_{G1} and V_{G2} . This would naturally give a combination of lengthening and sharpening. Investigating this effects in detail would require a more accurate confinement model, but we believe the gross effect of magnetic field on pump current accuracy is well captured by the above description.

We now address a distinct second effect of magnetic field on this system. In Ref 12 it was shown that the rapid changes in electrostatic confinement potential can populate excited states

of the dot by nonadiabatic processes [23]. Tunneling from excited states is more likely than from the ground state; electrons “spill” out of the pump and the current plateaux are eroded into a number of unquantised steps. This gives spectroscopic information about the dot states but destroys the accuracy of current quantization. We show here that these excitation features have a non-monotonic field dependence; excitations cannot be detected at low field but are also strongly suppressed at high field. This discovery has consequences for the ultimate accuracy of the quantum dot pump, but also acts to demonstrate the sensitivity of nonadiabatic processes to magnetic confinement.

Figure 3(a) shows $I(V_{G2})$ and dI/V_{G2} for $f = 1$ GHz, which is sufficiently high to induce excitations of the dot via nonadiabatic effects at intermediate fields. Excitation features emerge at modest fields of a few Tesla [12] but as the field is increased above 12 T these features (peaks in the derivative) become significantly weaker. This results in the recovery of accurate current quantization even when operating at higher frequencies. Figures 3(b), (c) shows this effect in more detail. The size of the field window where excitations are seen is of different size in different samples.

The observation of a range of fields where nonadiabatic effects are visible can be explained by a competition between magnetic and electrostatic effects on the electronic wavefunction. Nonadiabatic transition rates depend both on the strength and rapidity of the perturbation of the wavefunction [12, 24]. At high field $\omega_c \gg \omega_0$, the relative contribution to the confinement of the electrostatic component is diminished and the magnetic component determines the size of the wavefunction. Changes in the confinement potential during pumping have correspondingly weaker effects on the dot wavefunction and nonadiabatic transition rates will be reduced. Figures 3(d) and 3(e) show, for example, that the probability density $|\psi|^2$ and eigenenergy E_0 of the lowest energy orbital Fock-Darwin state become increasingly insensitive to changes in ω_0 at higher field. This is consistent with the disappearance of the excitation features at the highest fields.

A significant increase in the excitation gap between ground and excited states could be responsible for suppressing excitation effects at low field. A value of $\hbar\omega_0 \simeq 8$ meV at $B = 0$ has been found in these pumps previously [12] by fitting features in the pumped current to the energy differences $\Delta_n = E_n - E_0$ for Fock-Darwin eigenenergies $E_n(B)$ (here n is the radial quantum number). At higher field Δ_n is reduced but for the above value of ω_0 this variation is rather weak, with a drop of only 20% in an applied field of 2 T. If the excitation processes happen earlier in the pumping cycle, when the dot confinement is smaller, the field dependence of Δ_n is much stronger (see Fig. 3(f)). In this case the rapid rise in the excitation gap near zero field can cut off the excitation process as seen experimentally.

We have shown that electron dynamics in single-electron tunable-barrier pumps are sensitive to magnetic fields via two mechanisms; the time dependence of tunnel rates and by suppression of nonadiabatic transitions. These effects allow the

pumps operate with error rates smaller than a few parts in 10^6 at high field. This shows that this is a convenient system in which to study electron dynamics in high magnetic fields.

This research is supported by the UK Department for Business, Innovation and Skills, the European Metrology Research Programme, grant no. 217257, the UK EPSRC and Korea NRF (2009-0078437).

-
- [1] J. Elzerman, R. Hanson, L. van Beveren, B. Witkamp, L. Vandersypen, and L. Kouwenhoven, *Nature* **430**, 431 (2004).
 - [2] T. Hayashi, T. Fujisawa, H. Cheong, Y. Jeong, and Y. Hirayama, *Phys. Rev. Lett.* **91**, 226804 (2003).
 - [3] D. Loss and D. DiVincenzo, *Phys. Rev. A* **57**, 120 (1998).
 - [4] J. Shilton, V. Talyanskii, M. Pepper, D. Ritchie, J. Frost, C. Ford, C. Smith, and G. Jones, *J. Phys.-Condens. Matter* **8**, L531 (1996).
 - [5] M. D. Blumenthal, B. Kaestner, L. Li, S. Giblin, T. J. B. M. Janssen, M. Pepper, D. Anderson, G. Jones, and D. A. Ritchie, *Nat. Phys.* **3**, 343 (2007).
 - [6] A. Fujiwara, K. Nishiguchi, and Y. Ono, *Appl. Phys. Lett.* **92**, 042102 (2008).
 - [7] C. Darwin, in *Mathematical Proceedings of the Cambridge Philosophical Society* (Cambridge Univ Press, 1931), vol. 27, p. 86.
 - [8] S. Tarucha, D. Austing, T. Honda, R. vanderHage, and L. Kouwenhoven, *Phys. Rev. Lett.* **77**, 3613 (1996).
 - [9] M. Ciorga, A. Wensauer, M. Pioro-Ladriere, M. Korkusinski, J. Kyriakidis, A. Sachrajda, and P. Hawrylak, *Phys. Rev. Lett.* **88**, 256804 (2002).
 - [10] S. J. Wright, M. D. Blumenthal, G. Gumbs, A. L. Thorn, M. Pepper, T. J. B. M. Janssen, S. N. Holmes, D. Anderson, G. A. C. Jones, C. A. Nicoll, et al., *Phys. Rev. B* **78**, 233311 (2008).
 - [11] B. Kaestner, C. Leicht, V. Kashcheyevs, K. Pierz, U. Siegner, and H. W. Schumacher, *Appl. Phys. Lett.* **94**, 012106 (2009).
 - [12] M. Kataoka, J. D. Fletcher, P. See, S. P. Giblin, T. J. B. M. Janssen, J. P. Griffiths, G. A. C. Jones, I. Farrer, and D. A. Ritchie, *Phys. Rev. Lett.* **106**, 126801 (2011).
 - [13] In previous devices [5] an etched channel provided lateral confinement, whereas here the ‘cut-away’ region in the narrow finger gates (size 100 nm) creates a natural site for the formation of a few-electron quantum dot when negative voltages are applied to both gates.
 - [14] $V_{RF} \simeq V_{G1}$, $V_{G2} \simeq 0.4$ V.
 - [15] The device is always in a non-conducting state due to large exit gate potential barrier. Pumping takes place at nominally zero source-drain bias. The direction of the current is determined by the choice of modulated gate.
 - [16] Some values of V_{G1} lead to incomplete emptying of the dot. We consider the case when all of the electrons are emptied from the dot at the end of the cycle.
 - [17] S. J. Wright, A. L. Thorn, M. D. Blumenthal, S. P. Giblin, M. Pepper, T. J. B. M. Janssen, M. Kataoka, J. D. Fletcher, G. A. C. Jones, C. A. Nicoll, et al., *J. Appl. Phys.* **109**, 102422 (2011).
 - [18] This system uses a differential technique against a reference current calibrated with Josephson and Quantum Hall standards. Details will be published elsewhere.
 - [19] V. Kashcheyevs and B. Kaestner, *Phys. Rev. Lett.* **104**, 186805

- (2010).
- [20] H.-S. Sim, G. Ihm, N. Kim, and K. Chang, Phys. Rev. Lett. **87**, 146601 (2001).
- [21] S. Datta, *Electronic transport in mesoscopic systems* (Cambridge Univ Press, 1997), ISBN 0521599431.
- [22] Transverse confinement strength $\hbar\omega \simeq 4.9$ meV.
- [23] M. Born and V. Fock, Zeitschrift für Physik **51**, 165 (1928).
- [24] H. Lewis Jr and W. Riesenfeld, Journal of Mathematical Physics **10**, 1458 (1969).